

Fast Nonradiative Decay Paths in Organic Solar Cells: Implications for Designing More Efficient Photovoltaic Systems

Alessandro Landi*, Daniele Padula*, and Andrea Peluso*

Cite This: *ACS Appl. Energy Mater.* 2024, 7, 707–714

Read Online

ACCESS |



Metrics & More



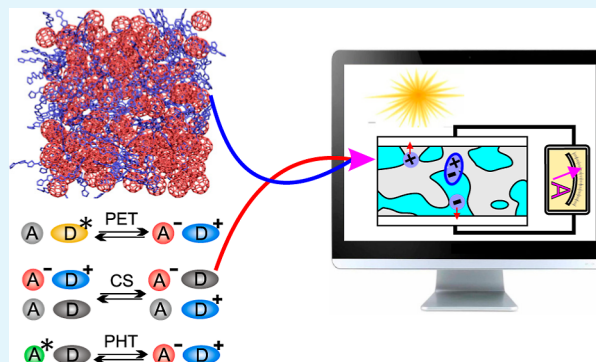
Article Recommendations



Supporting Information

ABSTRACT: With the aim of understanding the sources of energy losses in bulk heterojunction solar cells, the rates of elementary charge-transfer processes occurring at the donor–acceptor interface have been determined by employing a combined classical and quantum mechanical approach for four prototypical blends, covering a wide range of power conversion efficiency values. The results show that backward electron transfer from the charge-transfer state at the D/A interface to the ground state is a fast process, which can efficiently compete with charge dissociation; indeed, a clear-cut correlation between the rates of nonradiative charge recombination and the observed power conversion efficiency has been found. The finding presented above suggests important criteria for the rational design of acceptor–donor blends for organic photovoltaics.

KEYWORDS: organic solar cells, bulk heterojunctions, Fermi's golden rule, molecular dynamics, charge recombination, non-fullerene acceptors



INTRODUCTION

Photovoltaic solar cells (PSCs) are among the most promising technologies for renewable energy production. Great research efforts have been focused on organic solar cells (OSCs), which offer potential advantages over traditional silicon devices, because of their much lower costs, lower weight, improved mechanical properties, and chemically tunable electronic properties.^{1–5} The most commonly used architecture for OSCs is the bulk heterojunction (BHJ) one, where electron acceptor (A) and electron donor (D) domains interpenetrate each other, thus featuring a heterointerface distributed throughout the entire active layer,⁵ ensuring the required film thickness for sufficient radiation absorption while reducing the distance that excitons must travel to reach the D/A interface.⁶

The first organic solar cells were almost exclusively based on fullerene C60 (Figure 1) as an electron acceptor and were characterized by a low power conversion efficiency (PCE).⁷ Substantial improvements have been obtained by replacing C60 with PCBM (see Figure 1) as acceptor, since the latter exhibits higher electron mobility, better processability (the side chain makes it more soluble, useful to obtain a uniform morphology) and tunability of energy level alignment with donors.⁸ Further progresses were provided by a new class of donors, where a central electron-rich core is flanked by relatively electron-poor units and terminated with π -conjugated end-caps, with aliphatic side chains that improve processability.⁹ The electron-rich core allows for strong intramolecular charge transfer, thus broadening low-energy optical transitions and improving absorption, while

the two electron-poor units deepen the energy of the highest occupied molecular orbital (HOMO) and maintain high oxidation potentials. The high planarity of the π -system also improves charge carrier mobility by promoting delocalization and intermolecular stacking. Among the various members of this family, the small molecule indicated as DTS (Figure 1) led to a remarkable PCE up to 8.9% in blends with PC70BM.^{9–11} More recently, further PCE improvements have been obtained by the introduction of nonfullerene acceptors (NFAs), molecules formed by fused-ring structures composed of donor and acceptor moieties, which offer better stability and tunability than fullerenes.^{12–14} The first NFA, created by Zhan's team, with an A-D-A structure,¹⁵ led to PCEs up to 13%;^{16,17} higher efficiencies were attained with the introduction of acceptors having A-D-A'-D-A structures, in particular Y6,¹⁸ see Figure 1, which yielded a PCE higher than 18% for single-junction OSCs.^{19,20}

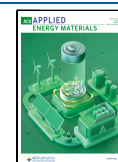
NFAs have been mostly used in blends with polymeric donors, frequently derivatives of polythiophene, which, however, exhibit poor batch-to-batch reproducibility, posing a significant obstacle to the commercialization of OSCs on a large

Received: November 5, 2023

Revised: December 13, 2023

Accepted: December 13, 2023

Published: December 28, 2023



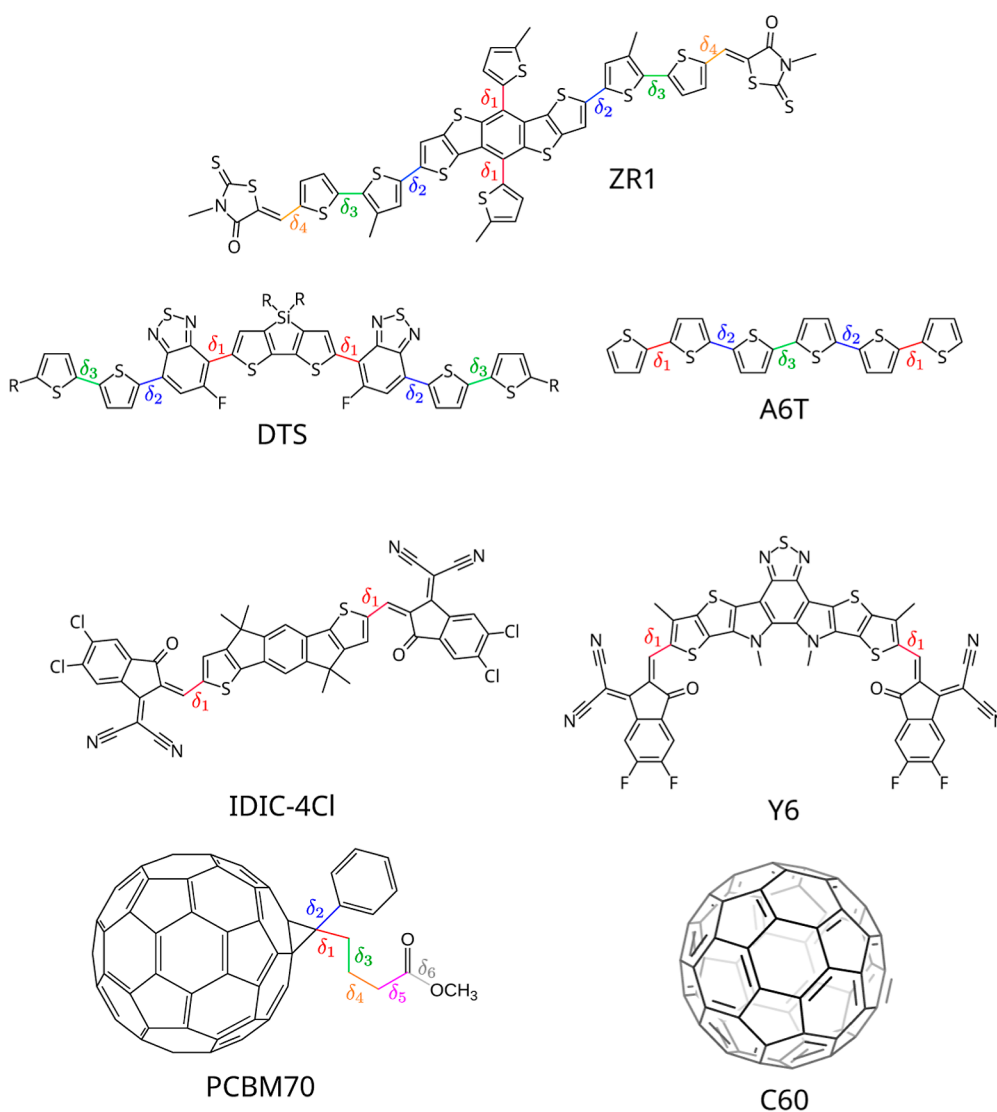


Figure 1. Structures of the molecules studied in this work. Top: 2,2':5',2'':5'',2''':5''',2''':5''''-sexithiophene (A6T in the text) and (C60-Ih)[5,6]fullerene (C60 in the text). Middle: 6-fluoro-4-(5'-hexyl-[2,2'-bithiophene]-5-yl) benzo[c][1,2,5]thiadiazolethieno(3,2-*b*; 2',3'-*d*)silole (DTS in the text) and [6,6]-phenyl-C71-butyric acid methyl ester (PCBM in the text). Bottom: 5,5'-[[4,8-bis[5-(2-butyloctyl)-2-thienyl]dithieno[2,3-*d*:2',3'-*d'*]benzo[1,2-*b*:4,5-*b'*]dithiophene-2,6-diyl]bis[3'-octyl[2,2'-bithiophene]-5'',5'-diyl]methylidyne]]bis[3-hexyl-2-thioxo-4-thiazolidinone] (ZR1 in the text) 2,2'-((2Z,2'Z)-((4,4,9,9-tetraoctyl-4,9-dihydro-*s*-indaceno[1,2-*b*:5,6-*b'*]dithiophene-2,7-diyl)bis(methanylylidene))bis(5,6-dichloro-3-oxo-2,3-dihydro-1*H*-indene-2,1-diylidene))dimalononitrile (IDIC in the text) 2,2'-((2Z,2'Z)-((12,13-bis(2-ethylhexyl)-3,9-diundecyl-12,13-dihydro-[1,2,5]thiadiazolo[3,4-*e*]thieno[2',3':4',5']thieno[2',3':4,5]pyrrolo[3,2-*g*]thieno[2',3':4,5]thieno[3,2-*b*]indole-2,10-diyl)bis(methanylylidene))bis(5,6-difluoro-3-oxo-2,3-dihydro-1*H*-indene-2,1-diylidene))dimalononitrile (Y6 in the text).

scale. To address this issue, extensive efforts have been devoted to design small-molecule donors,^{21–24} which have allowed to obtain PCEs up to 15%.²² In particular, in ref. 22, the archetypes of the two NFA families discussed above, i.e., IDIC and Y6, have been combined with the same small-molecule donor, ZR1 (see Figure 1), leading to a PCE of 9.64% for ZR1:IDIC and 14.34% for ZR1:Y6.²²

Despite these improvements, significant challenges must still be addressed for OSCs to reach the market. Indeed, despite high values of fill factors (FFs) and of external and internal quantum efficiencies obtained to date,^{25,26} PCE remains below the theoretical Shockley–Queisser limit of 33% for single-junction devices²⁷ and still significantly lower than those of inorganic cells, where efficiencies higher than 25% have been reported.²⁸ One of the primary reasons for this difference is the notably low open-circuit voltage (V_{oc}) of OSCs compared to the absorber

optical band gap (E_g). Studies on OSCs demonstrated that external quantum efficiency declines steeply when the energy loss, $E_{loss} = E_g - qV_{oc}$, is lower than 0.6 eV and that for the most efficient OSCs, E_{loss} is between 0.7 and 0.9 eV.^{29,30} In perovskite solar cells, E_{loss} is less than 0.5 eV,³¹ but any attempt to reduce E_{loss} in OSCs to less than 0.6 eV resulted in a significant drop in the quantum efficiency for charge generation, for reasons that are not yet well understood.

In a recent study, the performances of a set of about a hundred different D/A blends, used in both bulk heterojunction and planar heterojunction architectures, were analyzed.⁷ A clear correlation between V_{oc} and the energy of the charge-transfer (CT) state (E_{CT^-}) was observed: V_{oc} decreases as E_{CT^-} decreases for the entire range covered by the selected data (0.7 to 1.7 eV). Low V_{oc} can be attributed to both nonradiative and radiative decay pathways to the ground state. Because radiative decay is

unavoidable, suppression of the fast nonradiative decay paths could be an effective approach to enhance OSC performance, as it happened for GaAs devices.³²

It has been shown that many factors can be responsible of the lower V_{oc} which characterizes organic devices,³³ and energy loss can be mitigated by using very rigid small molecules, which could achieve a very low degree of energetic disorder.³⁴ In particular, the sources of nonradiative decay in organic solar cells appear to be one of the most urgent issue in OSC technology because efficient organic solar cells (18.93% certified) with reduced nonradiative recombination loss have been obtained by using a particular deposition strategy which could avoid excessive molecular aggregation, leading to the formation of more ordered molecular aggregates;³⁵ moreover, theoretical models have pointed out the importance of nonradiative recombination through the charge-transfer state.^{7,36}

Herein, to gain more insights into the factors that determine energy losses in OSCs, we studied four D/A blends, as reported in Figure 1. They have been chosen to (i) be representative of different ranges of efficiency and (ii) cover the history of development of BHJ solar cell materials, featuring different small-molecule donors and either fullerene or nonfullerene acceptors.

We have combined molecular dynamics (MD) simulations to obtain a realistic morphology,³⁷ and Fermi's Golden Rule (FGR) to determine the rates of several elementary charge-transfer processes that occur at the D/A interface; the results show that the main nonradiative decay path of the CT state is the backward electron transfer to the ground state and that there is a clear-cut correlation between the rates of this process and the observed PCE.

METHODS

Molecular Dynamics Simulations. To perform MD simulations of the D/A interface, we have first produced accurate intramolecular quantum-mechanically derived force field (QMD-FF) parametrization for all the molecules under study, adopting the JOYCE parametrization protocol,^{38,39} which exploits a fitting procedure of the Hessian matrix obtained at the DFT/B3LYP-D3/6-31G(d) level. Because in some of the molecules under study, a certain degree of flexibility should be expected for the rotation around alternating σ bonds, significant amplitude distortions from the equilibrium positions might take place, making the harmonic approximation unsuitable. Therefore, for each of the dihedrals δ shown in Figure 1, we have performed a relaxed internal energy scan, by optimizing all other degrees of freedom at the same level of theory (B3LYP-D3/6-31G(d)). It should be remarked that these are ground-state force field, thereby indicating that the nuclear relaxation effects occurring upon photon absorption are excluded from the model. This has been done because the MD is used to obtain a reliable morphology of the actual device, which is processed without external excitation during its creation. In the Supporting Information, an extensive description of the parametrization procedure has been reported. The description of the molecules for classical MD simulations has been completed by combining the intramolecular QMD-FFs with Lennard-Jones parameters from appropriate OPLS atom types,⁴⁰ and point charges fitted following the RESP procedure.⁴¹ The resulting force fields were made available to the community in a public GitHub repository.

Rate Calculation. The rates of elementary CT processes occurring at the D/A interface have been evaluated by Fermi's Golden Rule (FGR), whereby the transition rate between two electronic states li and lj , whose energy difference is ΔE , is expressed as

$$k_{ij} = \frac{2\pi}{\hbar} |J_{ij}|^2 F(\Delta E, T) \quad (1)$$

Here, J_{ij} is the electronic coupling element and $F(\Delta E, T)$ is the Franck–Condon weighted density of states (FCWD), averaged over a thermal equilibrium distribution of initial vibrational states

$$F(\Delta E, T) = \sum_{v'} \sum_{v''} w_{v'}(T) |\langle v' | v'' \rangle|^2 \delta(E_{v'} - E_{jv''} - \Delta E_{ji}) \\ = |V_{ji}|^2 \rho(\Delta E, T) \quad (2)$$

where v' and v'' denote the vectors of the vibrational quantum states of i and j , respectively, and w_v is the equilibrium (Boltzmann) population of liv' .

By using Kubo's generating function approach,⁴² the infinite summations appearing in eq 2 can be avoided in the harmonic approximation of nuclear motions,^{42–45} allowing for an effective evaluation of $F(\Delta E, T)$, which takes into account both the effects of equilibrium position displacements and normal mode mixing upon transition, and includes the whole sets of nuclear normal modes of vibrations.^{42,45–48} Because the approach is full dimensional in the space of nuclear coordinates, the limitation imposed by the harmonic approximation is not expected to be too serious, inasmuch as highly excited vibrational states are not expected to significantly contribute to $F(\Delta E, T)$ because of their comparatively lower Franck–Condon factors. Because our approach includes the whole set of intramolecular coordinates of both the acceptor and the donor, the energy difference between the initial and final states is likely to be distributed over a large number of displaced modes, each with a low quantum number. Indeed the approach adopted here proved to yield extremely reliable rates both of radiative and nonradiative electronic transitions:^{39,49–54} among these, we remark an excellent agreement obtained for intersystem crossing in benzophenone.⁵⁵

RESULTS AND DISCUSSION

With the intent of relating the performances of the four BHJ blends to the rates of elementary processes occurring at the D/A interface, we have considered the following processes: (i) photoinduced electron transfer (PET), in which an electron is transferred from the LUMO of D in its excited state (D^*) to the empty LUMO of A, leading to D^+A^- ; (ii) photoinduced hole transfer (PHT), in which an electron is transferred from the HOMO of D to the lowest energy SOMO of A^* , leading also to D^+A^- ; (iii) exciton energy transfer (EET), in which energy is transferred from D^* to A^* ; (iv) charge recombination (CR) from the D^+A^- charge transfer (CT) state to the neutral ground state. Herein, we have not considered the involvement of triplet states,^{56,57} whose possible role has been discussed in a previous paper,⁵⁶ which is not of crucial interest here, where we focus on understanding the sources of energy loss in BHJ rather than on the mechanisms of charge dissociation which could take place in devices. All processes are schematized below:

- $D^* + A \rightarrow D^+A^-$ (PET);
- $D + A^* \rightarrow D^+A^-$ (PHT);
- $D^* + A \rightarrow D + A^*$ (EET);
- $D^+A^- \rightarrow D + A$ (CR).

The D/A interface has been characterized at the classical level of theory, performing molecular dynamics simulations for all the four blends considered in this work. We have randomly arranged an appropriate number of donor and acceptor molecules (64 for each) in a cubic box, which is in line with the adopted experimental ratio.²² After a 1 ns equilibration and 100 ns of simulated annealing, all of the blends assume random arrangements, except DTS:PC70BM, for which MD simulations starting from a random arrangement lead to unphysical morphologies. For this blend we have adopted an alternative approach,⁵⁸ consisting in a preliminary deposition step by creating a $3 \times 3 \times 3$ supercell of PCBM70 (taken from the X-ray

Table 1. Average Electronic Couplings (J , Absolute Values) and Rate Constants (k), Energy Differences, and Reorganization Energies of Donor (λ^D) and Acceptor (λ^A) for Each of the Processes Occurring at the D/A Interface^a

	J (meV)	ΔE (meV)	k (s ⁻¹)	λ^D (meV)	λ^A (meV)	J (meV)	ΔE^c (meV)	k (s ⁻¹)	λ^D (meV)	λ^A (meV)
			A6T:C60					DTS:PC70BM ^b		
PET	12.6	-406.5	2.25×10^{12}	94	66	7.7	-128.3	7.65×10^{11}	75	
PHT	12.5	-217	8.22×10^{11}	136	132	6.3	-438.8	5.62×10^{11}	112	
CR	14.1	-1625	7.24×10^{11}	168	65	7.0	-1432	2.50×10^{11}	119	
EET	0.6	-99.3	8.41×10^8	356	251	1.3	+410.6	2.33×10^{10}	188	
			ZR1:IDIC					ZR1:Y6		
PET	4.6	-371.4	8.00×10^{11}	81	92	5.4	-206.5	4.06×10^{12}	81	59
PHT	4.0	+232.0	6.25×10^{11}	80	110	5.8	-113.0	9.25×10^{11}	80	111
CR	4.8	-1288	3.00×10^{11}	87	85	6.6	-1452	4.65×10^{10}	87	60
EET	8.1	-21.8	3.17×10^{10}	174	71	8.2	-93.5	9.80×10^{11}	174	56

^aEnergy differences include a binding energy of 0.1 eV for k evaluations.^{12,67} The standard deviation of the average electronic coupling is of the same order of magnitude as the electronic couplings themselves, as typically found in these systems.^{65,68} ^bReferring to the reverse exergonic process.

^cExperimental data ref 56.

structure), and depositing on it an equal number of DTS molecules (i.e., 108). The deposition dynamics last 250 ps per molecule, with a 1 fs integration time step. The results of these preliminary MD simulations are shown in Figure S1 of the Supporting Information.

After simulated annealing, trajectories were propagated for 100 ns, sampling ca 150 D/A pairs geometries from the last 40 ns of each simulation. For each of them, we have evaluated the electronic coupling elements for the processes cited above, using the structure as retrieved from MD; indeed, further structural refinements are not needed, as a consequence of the force field QM parametrization. For PET, PHT, and CR, the frontier orbital approach has been adopted,⁵⁹ whereas EET couplings have been calculated through a perturbative approach from the transition densities of the noninteracting units.^{60,61} More details are provided in the Supporting Information. The rate constants of the four processes above have then been obtained by eqs 1 and 2; the results have been averaged over all the sampled pairs and reported in Table 1, together with average electronic couplings.

The calculation of $F(\Delta E, T)$ has been carried out by assuming that vibrational motions within each molecule are independent from each other, which allows us to evaluate the Franck–Condon weighted density of states of the whole process by the convolution of those pertaining to the two half-processes. For instance, for an ET process from D to A, the density of states of the whole process has been evaluated as

$$F(\Delta E, T) = \int_{-\infty}^{\infty} dE \mathcal{D}(E) \mathcal{A}(\Delta E - E) \quad (3)$$

where $\mathcal{D}(E)$ and $\mathcal{A}(E)$ are the FCWDs of the two half reactions: $D \rightarrow e^- + D^+$ and $A + e^- \rightarrow A^-$, respectively. Apart from simplifying calculations, the above approximation also allows one to have control over the computed quantities that determine the resulting FCWDs: indeed $\mathcal{D}(E)$ is the electron removal spectral distribution of the donor molecule and $\mathcal{A}(E)$ is the electron attachment spectral distribution of the acceptor,^{45,62} quantities which are both experimentally accessible.^{63,64} In the Supporting Information, we reported a comparison between predicted and observed $\mathcal{A}(E)$ of C60, the only molecule among those considered here for which the experimental photoelectron spectrum of the anion is available. $F(\Delta E, T)$ is evaluated at the minimum energy conformation⁴⁵ because it is assumed that the

conformation (and the environment) has a little impact on the frequencies. The average values of the computed electronic couplings and of the rates of each physical process considered here are reported in Table 1. It should be remarked that we have not used an average electronic coupling for the subsequent rate calculation; rather, we have computed the rate for each electronic coupling value. This resulted in ca 600 rates, which cannot be all reported here. Instead, we have computed and shown in Table 1 the average electronic coupling and the average rate for each physical process discussed in this work, as a figure of merit for comparing different blends. Even though the distributions are somewhat large, this approach is not only justified in these complicated materials for understanding purposes but also widely used in the current literature.^{65,66}

Inspection of Table 1 shows that average transfer integrals are quite similar for all the D/A pairs under study, with the notable exception of A6T:C60, which exhibits significantly higher values of the electronic couplings for PET, PHT, and CR. That can be explained on the basis of two factors: (i) both A6T and C60 are comparatively smaller molecules and (ii) they do not bear any alkyl chain substituents. Both factors ensure a better packing, leading to higher couplings. Notwithstanding, A6T:C60 is the worst performing blend, exhibiting a very modest PCE ($\approx 1\%$).⁷ Our computations predict for this D/A pair the highest CR rate ($\approx 7 \times 10^{11}$), despite the backward ET process from the CT state D^+A^- to the ground state (GS) being highly exergonic ($\Delta E = -1.6$ eV), exhibiting the largest energy change among the four blends considered here. Our analysis also shows that the slowest CR rate ($k_{CR} = 4 \times 10^{10}$) pertains to the most performing pair ZR1:Y6, having PCE ca 14%,²² whereas for ZR1:IDIC and DTS:PC70BM, whose performances in terms of PCE are similar, ca 9%, the rates of charge recombination to the ground state are also similar to each other: 3.0×10^{11} and 2.5×10^{11} , respectively.

Those results indicate that CR rates and observed PCEs could be strongly related to each other and, indeed, by reporting the observed PCEs as a function of predicted charge recombination rates, a quasi-linear relation between the two quantities is found, see Figure 2.

We remark that this correlation should not be intended as an equation to predict the PCE of solar cells. The main goal of our study is to show pictorially the existence of a relationship between PCE and the charge recombination rate (which is linear in the interval of PCE examined). None of the other predicted

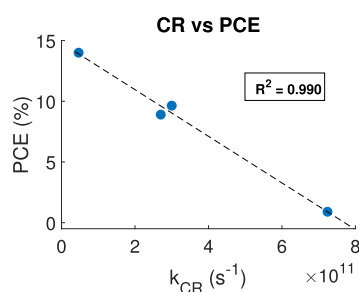


Figure 2. PCE as a function of the CR rate. The dashed line represent the best linear fitting, with $R^2 = 0.99$.

rates exhibit such a clear correlation with the observed PCEs, suggesting that the progress in PCEs over the years could be related to slowing down charge recombination processes. Indeed, CR rates have a great impact on the lifetime of the CT state at the D/A interface, as it can be judged by the predicted time populations of the relevant electronic states, D^* , A^* , A^-D^+ (CT), and ground state (GS), at the D/A interface, calculated by employing the Pauli master equation approach,⁶⁹ with the rate constants of Table 1 and the initial condition $P_D^* = 1$ at $t = 0$. The results are reported in Figure 3 for all of the D/A pairs (details of calculations are reported in the Supporting Information).

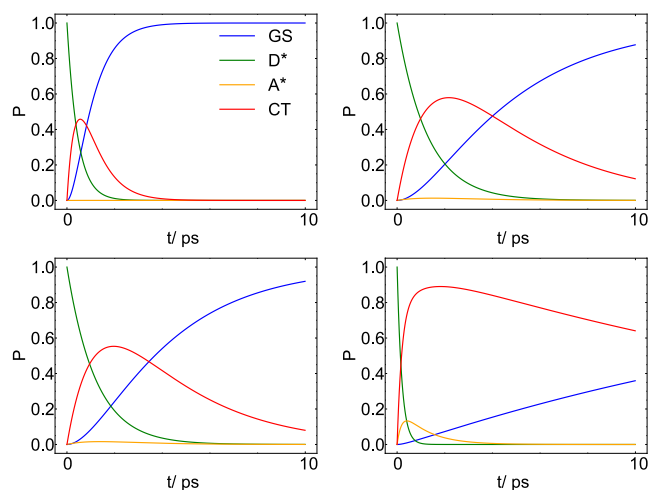


Figure 3. Electronic state population dynamics evolved according to the equations reported in the Supporting Information for A6T:C60 (top left), DTS:PCBM (top right), ZR1:IDIC (bottom left), and ZR1:Y6 (bottom right).

Inspection of Figure 3 shows that for the least performing blend, the maximum population of the CT state is significantly lower (~ 0.4) than for the other pairs; most importantly, the CT state, which gives rise to charge dissociation, is the predominant one only in a very short time interval, lasting less than a picosecond. Vice versa, for the most performing blend, the CT state reaches a much higher population (~ 0.9) and exhibits a much longer lifetime, being the predominant state in almost the whole investigated time interval.

Figure 3 undoubtedly shows that, at least for the four blends investigated here, the rates of the backward electron transfer from the CT state to the ground state can play a crucial role in device performances. Because the computed electronic couplings of the three most performing blends are very similar to each other, the origin of the different CR rates must be found

in the other two factors which determine them: the energy differences between the initial and final states and the Franck–Condon weighted density of states.

In Figure 4, the $F(\Delta E, T)$ for the nonradiative decay to the ground state via backward ET are reported as a function of ΔE . The most performing blends exhibit the narrowest $F(\Delta E, T)$, thus making CR rates decay rapidly as ΔE increases. The shape of $F(\Delta E, T)$ as a function of ΔE appears to play an important role; in the classical Marcus' picture of ET, the Franck–Condon density of states is approximated by a Gaussian function, whose peak and width depend on the ΔG and the reorganization energy of the ET reaction. The $F(\Delta E, T)$ numerically computed here via eq 2 have no Gaussian shape, but their widths and maximum locations clearly depend on the reorganization energies associated with the two-half redox reactions and on the vibrational frequencies of the displaced modes. Inspection of Table 1 shows that the high CR rates of the A6T:C60 blend is associated with a large reorganization energy of the donor, which makes the corresponding FCWD a broad function of the energy difference. Vice versa, the most performing ZR1:Y6 pair exhibits lower CR rates because of its narrow FCWD, due to the low reorganization energies of both D and A.

Interestingly, a small decrease of the reorganization energy of one redox partner provides a significant narrowing of the FCWD; that is an encouraging result, showing that there is still room for further PCE improvements.

CONCLUSIONS

We have provided convincing evidence that the main source of energy losses in organic BHJ solar cells lies in fast electron transfer from the CT state D^+A^- to the ground state. With some notable exceptions,⁷ charge recombination to the ground state has been largely overlooked in the past because it was expected to be slow on the basis of the well-known energy gap rule; herein, we have shown that it can occur on subnanosecond time scales, being thus significantly faster than radiative decay. Fast decay of interfacial singlet CT states via back electron transfer to the ground state is expected to characterize almost all D/A pairs because an overlap between D and A frontier orbitals is needed for ensuring efficient and fast photoinduced electron transfer. The present finding thus opens new routes to a rational design of donor-acceptor blends for organic photovoltaics: the combined optimization of the two parameters that control charge recombination rates, *i.e.*, the energy difference between the charge separated and ground states and the width of the Franck–Condon density of states, can pave the way for substantial improvements in OPV efficiency. The task is, however, not so easy because the D/A pairs considered here exhibit already small reorganization energies, and increasing the optical band gap of D and/or A to push up the energy of the CT state is limited by the spectral distribution of the solar spectrum. Notwithstanding, our results suggest that further efforts along this route are worthwhile, inasmuch as we have shown that a small decrease in the reorganization energies can result in a significant narrowing of the corresponding Franck–Condon density of states. The computational protocol adopted here enables the facile computation of CR rates, at the reasonable cost of four energy optimizations, allowing for a rapid screening of materials databases to identify novel photovoltaic organic materials, with favorable charge recombination rates (see the Supporting Information for a discussion of the computational cost). Of course, other routes have to be pursued; among them, slowing down charge recombination via formation of a triplet

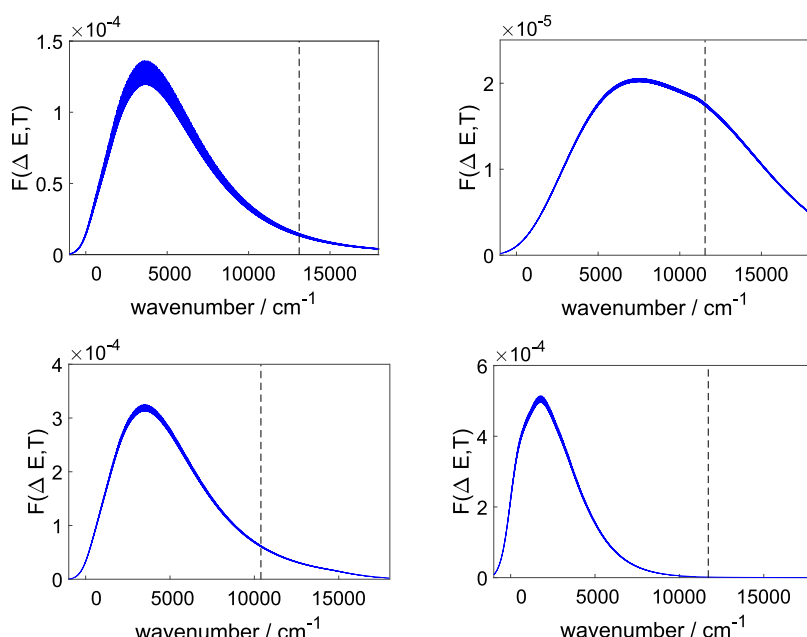


Figure 4. Franck–Condon weighted densities of states at $T = 298$ K as a function of the energy difference from the initial and final states for charge recombination occurring at the D/A interface. In clockwise order: A6T:C60; DTS:PCBM; ZR1:Y6; ZR1:IDIC. The dashed line indicates the ΔE of the transition.

CT state at the D/A interface appears to be a promising one.⁵⁶ In light of a very recent report,⁷⁰ showing that BHJ solar cell devices can display high performances (efficiency >18%) and stability close to a commercial level (lifetime $t_{80\%} \approx 8500$ h), we hope that the insights into the solar cell performances provided by our computational protocol could be of great help in the quest toward making OPVs a commercially viable technology in the near future.

■ ASSOCIATED CONTENT

SI Supporting Information

The Supporting Information is available free of charge at <https://pubs.acs.org/doi/10.1021/acsaem.3c02790>.

Computational Details; FCWDs for the rates in Table 1 not shown in Figure 4; comparison between experimental and predicted energies; comparison between experimental and computed photoelectron spectrum for C₆₀; and details about the master equation approach (PDF)

■ AUTHOR INFORMATION

Corresponding Authors

Alessandro Landi – Dipartimento di Chimica e Biologia Adolfo Zambelli, Università di Salerno, I-84084 Salerno, Italy;
 orcid.org/0000-0003-3627-5535; Email: alelandi1@unisa.it

Daniele Padula – Dipartimento di Biotecnologie, Chimica e Farmacia, Università di Siena, I-53100 Siena, Italy;
 orcid.org/0000-0002-7171-7928;
 Email: daniele.padula@unisi.it

Andrea Peluso – Dipartimento di Chimica e Biologia Adolfo Zambelli, Università di Salerno, I-84084 Salerno, Italy;
 orcid.org/0000-0002-6140-9825; Email: apeluso@unisa.it

Complete contact information is available at:
<https://pubs.acs.org/10.1021/acsaem.3c02790>

Notes

The authors declare no competing financial interest.

■ ACKNOWLEDGMENTS

The financial support of Università degli Studi di Salerno is gratefully acknowledged. A.L. gratefully acknowledges the support funding from the Italian Ministry of University and Research (MUR, PRIN grant 2022XSC9P5). A.L. gratefully acknowledges computational resources kindly provided by the University of Liverpool. D.P. gratefully acknowledges funding from the Italian Ministry of University and Research (MUR, Rita Levi Montalcini grant PGR18PJMBW) and Università di Siena (F-CUR research support contribution).

■ REFERENCES

- (1) Hedley, G. J.; Ruseckas, A.; Samuel, I. D. W. Light Harvesting for Organic Photovoltaics. *Chem. Rev.* **2017**, *117*, 796–837.
- (2) Landi, A.; Peluso, A.; Troisi, A. Quantitative Prediction of the Electro-Mechanical Response in Organic Crystals. *Adv. Mater.* **2021**, *33*, 2008049.
- (3) Landi, A.; Reisjalali, M.; Elliott, J. D.; Matta, M.; Carbone, P.; Troisi, A. Simulation of polymeric mixed ionic and electronic conductors with a combined classical and quantum mechanical model. *J. Mater. Chem. C* **2023**, *11*, 8062–8073.
- (4) Landi, A.; Padula, D. Optimising Conformational Effects on Thermally Activated Delayed Fluorescence. *J. Mater. Chem. C* **2022**, *10*, 10699–10707.
- (5) Sun, J.; Ma, X.; Zhang, Z.; Yu, J.; Zhou, J.; Yin, X.; Yang, L.; Geng, R.; Zhu, R.; Zhang, F.; Tang, W. Dithieno[3,2-b:2',3'-d]pyrrol Fused Nonfullerene Acceptors Enabling Over 13% Efficiency for Organic Solar Cells. *Adv. Mater.* **2018**, *30*, 1707150.
- (6) Yeh, N.; Yeh, P. Organic Solar Cells: Their Developments and Potentials. *Renewable Sustainable Energy Rev.* **2013**, *21*, 421–431.
- (7) Benduhn, J.; Tvingstedt, K.; Piersimoni, F.; Ullbrich, S.; Fan, Y.; Tropiano, M.; McGarry, K. A.; Zeika, O.; Riede, M. K.; Douglas, C. J.; Barlow, S.; Marder, S. R.; Neher, D.; Spoltore, D.; Vandewal, K. Intrinsic non-radiative voltage losses in fullerene-based organic solar cells. *Nat. Energy* **2017**, *2*, 17053.

- (8) Chu, C.-W.; Shrotriya, V.; Li, G.; Yang, Y. Tuning acceptor energy level for efficient charge collection in copper-phthalocyanine-based organic solar cells. *Appl. Phys. Lett.* **2006**, *88*, 153504.
- (9) Sun, Y.; Welch, G. C.; Leong, W. L.; Takacs, C. J.; Bazan, G. C.; Heeger, A. J. Solution-Processed Small-Molecule Solar Cells with 6.7% Efficiency. *Nat. Mater.* **2012**, *11*, 44–48.
- (10) Kyaw, A. K. K.; Wang, D. H.; Wynands, D.; Zhang, J.; Nguyen, T.-Q.; Bazan, G. C.; Heeger, A. J. Improved Light Harvesting and Improved Efficiency by Insertion of an Optical Spacer (ZnO) in Solution-Processed Small-Molecule Solar Cells. *Nano Lett.* **2013**, *13*, 3796–3801.
- (11) Collins, S. D.; Proctor, C. M.; Ran, N. A.; Nguyen, T.-Q. Understanding Open-Circuit Voltage Loss through the Density of States in Organic Bulk Heterojunction Solar Cells. *Adv. Energy Mater.* **2016**, *6*, 1501721.
- (12) Wang, H.; Cao, J.; Yu, J.; Zhang, Z.; Geng, R.; Yang, L.; Tang, W. Molecular Engineering of Central Fused-Ring Cores of non-Fullerene Acceptors for High-Efficiency Organic Solar Cells. *J. Mater. Chem. A* **2019**, *7*, 4313–4333.
- (13) Padula, D.; Landi, A.; Prampolini, G. Assessing alkyl side chain effects on electron transport properties of Y6-derived non-fullerene acceptors. *Energy Adv.* **2023**, *2*, 1215–1224.
- (14) Zhao, Z.-W.; Omar, O. H.; Padula, D.; Geng, Y.; Troisi, A. Computational Identification of Novel Families of Nonfullerene Acceptors by Modification of Known Compounds. *J. Phys. Chem. Lett.* **2021**, *12*, 5009–5015.
- (15) Lin, Y.; Wang, J.; Zhang, Z.-G.; Bai, H.; Li, Y.; Zhu, D.; Zhan, X. An Electron Acceptor Challenging Fullerenes for Efficient Polymer Solar Cells. *Adv. Mater.* **2015**, *27*, 1170–1174.
- (16) Cui, Q.; Hu, Y.; Zhou, C.; Teng, F.; Huang, J.; Zhugayevych, A.; Tretiak, S.; Nguyen, T.-Q.; Bazan, G. C. Single Crystal Microwires of p-DTS(FBTTh₂)₂ and Their Use in the Fabrication of Field-Effect Transistors and Photodetectors. *Adv. Funct. Mater.* **2018**, *28*, 1702073.
- (17) Forti, G.; Nitti, A.; Osw, P.; Bianchi, G.; Po, R.; Pasini, D. Recent Advances in Non-Fullerene Acceptors of the IDIC/ITIC Families for Bulk-Heterojunction Organic Solar Cells. *Int. J. Mol. Sci.* **2020**, *21*, 8085.
- (18) Feng, L.; Yuan, J.; Zhang, Z.; Peng, H.; Zhang, Z.-G.; Xu, S.; Liu, Y.; Li, Y.; Zou, Y. Thieno[3,2-b]pyrrolo-Fused Pentacyclic Benzotriazole-Based Acceptor for Efficient Organic Photovoltaics. *ACS Appl. Mater. Interfaces* **2017**, *9*, 31985–31992.
- (19) Chen, J.; Cao, J.; Liu, L.; Xie, L.; Zhou, H.; Zhang, J.; Zhang, K.; Xiao, M.; Huang, F. Layer-by-Layer Processed PM6:Y6-Based Stable Ternary Polymer Solar Cells with Improved Efficiency over 18% by Incorporating an Asymmetric Thieno[3,2-b]indole-Based Acceptor. *Adv. Funct. Mater.* **2022**, *32*, 2200629.
- (20) Li, M.; Lin, H.; Ma, B.; Yu, X.; Du, X.; Yang, G.; Zheng, C.; Tao, S. Non-fullerene acceptor alloy strategy enabling stable ternary polymer solar cells with efficiency of 17.74%. *J. Mater. Chem. C* **2022**, *10*, 3207–3216.
- (21) Zhou, Z.; Xu, S.; Song, J.; Jin, Y.; Yue, Q.; Qian, Y.; Liu, F.; Zhang, F.; Zhu, X. High-efficiency small-molecule ternary solar cells with a hierarchical morphology enabled by synergizing fullerene and non-fullerene acceptors. *Nat. Energy* **2018**, *3*, 952–959.
- (22) Zhou, R.; Jiang, Z.; Yang, C.; Yu, J.; Feng, J.; Adil, M. A.; Deng, D.; Zou, W.; Zhang, J.; Lu, K.; Ma, W.; Gao, F.; Wei, Z. All-small-molecule organic solar cells with over 14% efficiency by optimizing hierarchical morphologies. *Nat. Commun.* **2019**, *10*, 5393.
- (23) Parisi, E.; Landi, A.; Fusco, S.; Manfredi, C.; Peluso, A.; Wahler, S.; Klapötke, T. M.; Centore, R. High-Energy-Density Materials: An Amphoteric N-Rich Bis(triazole) and Salts of Its Cationic and Anionic Species. *Inorg. Chem.* **2021**, *60*, 16213–16222.
- (24) Miao, J.; Meng, B.; Ding, Z.; Liu, J.; Wang, L. Organic solar cells based on small molecule donors and polymer acceptors operating at 150 °C. *J. Mater. Chem. A* **2020**, *8*, 10983–10988.
- (25) Park, S. H.; Roy, A.; Beaupré, S.; Cho, S.; Coates, N.; Moon, J. S.; Moses, D.; Leclerc, M.; Lee, K.; Heeger, A. J. Bulk heterojunction solar cells with internal quantum efficiency approaching 100%. *Nat. Photonics* **2009**, *3*, 297–302.
- (26) Liu, Y.; Zhao, J.; Li, Z.; Mu, C.; Ma, W.; Hu, H.; Jiang, K.; Lin, H.; Ade, H.; Yan, H. Aggregation and Morphology Control Enables Multiple Cases of High-Efficiency Polymer Solar Cells. *Nat. Commun.* **2014**, *5*, 5293.
- (27) Shockley, W.; Queisser, H. J. Detailed Balance Limit of Efficiency of p-n Junction Solar Cells. *J. Appl. Phys.* **1961**, *32*, 510–519.
- (28) Yoshikawa, K.; Kawasaki, H.; Yoshida, W.; Irie, T.; Konishi, K.; Nakano, K.; Uto, T.; Adachi, D.; Kanematsu, M.; Uzu, H.; Yamamoto, K. Silicon heterojunction solar cell with interdigitated back contacts for a photoconversion efficiency over 26%. *Nat. Energy* **2017**, *2*, 17032.
- (29) Li, W.; Hendriks, K. H.; Furlan, A.; Wienk, M. M.; Janssen, R. A. J. High Quantum Efficiencies in Polymer Solar Cells at Energy Losses below 0.6 eV. *J. Am. Chem. Soc.* **2015**, *137*, 2231–2234.
- (30) Menke, S. M.; Ran, N. A.; Bazan, G. C.; Friend, R. H. Understanding Energy Loss in Organic Solar Cells: Toward a New Efficiency Regime. *Joule* **2018**, *2*, 25–35.
- (31) Nayak, P. K.; Cahen, D. Updated Assessment of Possibilities and Limits for Solar Cells. *Adv. Mater.* **2014**, *26*, 1622–1628.
- (32) Queisser, H. J. Detailed balance limit for solar cell efficiency. *Mater. Sci. Eng., B* **2009**, *159–160*, 322–328.
- (33) Liu, Q.; Vandewal, K. Understanding and Suppressing Non-Radiative Recombination Losses in Non-Fullerene Organic Solar Cells. *Adv. Mater.* **2023**, *35*, 2302452.
- (34) Liu, S.; Yuan, J.; Deng, W.; Luo, M.; Xie, Y.; Liang, Q.; Zou, Y.; He, Z.; Wu, H.; Cao, Y. High-efficiency organic solar cells with low non-radiative recombination loss and low energetic disorder. *Nat. Photonics* **2020**, *14*, 300–305.
- (35) Fu, J.; Fong, P. W. K.; Liu, H.; Huang, C.-S.; Lu, X.; Lu, S.; Abdelsamie, M.; Kodalle, T.; Sutter-Fella, C. M.; Yang, Y.; Li, G. 19.31% binary organic solar cell and low non-radiative recombination enabled by non-monotonic intermediate state transition. *Nat. Commun.* **2023**, *14* (1), 1760.
- (36) Azzouzi, M.; Yan, J.; Kirchartz, T.; Liu, K.; Wang, J.; Wu, H.; Nelson, J. Nonradiative Energy Losses in Bulk-Heterojunction Organic Photovoltaics. *Phys. Rev. X* **2018**, *8*, 031055.
- (37) Long, G.; Li, A.; Shi, R.; Zhou, Y.-C.; Yang, X.; Zuo, Y.; Wu, W.-R.; Jeng, U.-S.; Wang, Y.; Wan, X.; Shen, P.; Zhang, H.-L.; Yan, T.; Chen, Y. The Evidence for Fullerene Aggregation in High-Performance Small-Molecule Solar Cells by Molecular Dynamics Simulation. *Adv. Electron. Mater.* **2015**, *1*, 1500217.
- (38) Cerezo, J.; Prampolini, G.; Cacelli, I. Developing accurate intramolecular force fields for conjugated systems through explicit coupling terms. *Theor. Chem. Acc.* **2018**, *137*, 80.
- (39) Landi, A.; Padula, D. Multiple Charge Separation Pathways in New-Generation Non-Fullerene Acceptors: a Computational Study. *J. Mater. Chem. A* **2021**, *9*, 24849–24856.
- (40) Jorgensen, W. L.; Maxwell, D. S.; Tirado-Rives, J. Development and Testing of the OPLS All-Atom Force Field on Conformational Energetics and Properties of Organic Liquids. *J. Am. Chem. Soc.* **1996**, *118*, 11225–11236.
- (41) Bayly, C. I.; Cieplak, P.; Cornell, W.; Kollman, P. A. A well-behaved electrostatic potential based method using charge restraints for deriving atomic charges: the RESP model. *J. Phys. Chem.* **1993**, *97*, 10269–10280.
- (42) Kubo, R.; Toyozawa, Y. Application of the Method of Generating Function to Radiative and Non-Radiative Transitions of a Trapped Electron in a Crystal. *Prog. Theor. Phys.* **1955**, *13*, 160–182.
- (43) Landi, A. Charge Mobility Prediction in Organic Semiconductors: Comparison of Second-Order Cumulant Approximation and Transient Localization Theory. *J. Phys. Chem. C* **2019**, *123*, 18804–18812.
- (44) Landi, A.; Capobianco, A.; Peluso, A. Coherent Effects in Charge Transport in Molecular Wires: Toward a Unifying Picture of Long-Range Hole Transfer in DNA. *J. Phys. Chem. Lett.* **2020**, *11*, 7769–7775.
- (45) Borrelli, R.; Peluso, A. Elementary Electron Transfer Reactions: From Basic Concepts to Recent Computational Advances. *Comput. Mol. Biosci.* **2013**, *3*, 542–559.

- (46) Lax, M. The Franck-Condon Principle and Its Application to Crystals. *J. Chem. Phys.* **1952**, *20*, 1752–1760.
- (47) Landi, A.; Borrelli, R.; Capobianco, A.; Velardo, A.; Peluso, A. Hole Hopping Rates in Organic Semiconductors: A Second-Order Cumulant Approach. *J. Chem. Theory Comput.* **2018**, *14*, 1594–1601.
- (48) Wang, L.; Nan, G.; Yang, X.; Peng, Q.; Li, Q.; Shuai, Z. Computational Methods for Design of Organic Materials with High Charge Mobility. *Chem. Soc. Rev.* **2010**, *39*, 423–434.
- (49) Peng, Q.; Yi, Y.; Shuai, Z.; Shao, J. Toward Quantitative Prediction of Molecular Fluorescence Quantum Efficiency: Role of Duschinsky Rotation. *J. Am. Chem. Soc.* **2007**, *129*, 9333–9339.
- (50) Landi, A.; Borrelli, R.; Capobianco, A.; Velardo, A.; Peluso, A. Second-Order Cumulant Approach for the Evaluation of Anisotropic Hole Mobility in Organic Semiconductors. *J. Phys. Chem. C* **2018**, *122*, 25849–25857.
- (51) Velardo, A.; Borrelli, R.; Capobianco, A.; Landi, A.; Peluso, A. Disentangling Electronic and Vibrational Effects in the Prediction of Band Shapes for Singlet-Triplet Transitions. *J. Phys. Chem. C* **2019**, *123*, 14173–14179.
- (52) Niu, Y.; Peng, Q.; Deng, C.; Gao, X.; Shuai, Z. Theory of Excited State Decays and Optical Spectra: Application to Polyatomic Molecules. *J. Phys. Chem. A* **2010**, *114*, 7817–7831.
- (53) Landi, A.; Troisi, A.; Peluso, A. Explaining Different Experimental Hole Mobilities: Influence of Polymorphism on Dynamic Disorder in Pentacene. *J. Mater. Chem. C* **2019**, *7*, 9665–9670.
- (54) Marian, C. M. Spin-orbit Coupling and Intersystem Crossing in Molecules. *Wiley Interdiscip. Rev.: Comput. Mol. Sci.* **2012**, *2*, 187–203.
- (55) Velardo, A.; Landi, A.; Borrelli, R.; Peluso, A. Reliable Predictions of Benzophenone Singlet-Triplet Transition Rates: A Second-Order Cumulant Approach. *J. Phys. Chem. A* **2021**, *125*, 43–49.
- (56) Landi, A.; Landi, A.; Velardo, A.; Peluso, A. Efficient Charge Dissociation of Triplet Excitons in Bulk Heterojunction Solar Cells. *ACS Appl. Energy Mater.* **2022**, *5*, 10815–10824.
- (57) González, D. M.; Körstgens, V.; Yao, Y.; Song, L.; Santoro, G.; Roth, S. V.; Müller-Buschbaum, P. Improved Power Conversion Efficiency of P3HT:PCBM Organic Solar Cells by Strong Spin-Orbit Coupling-Induced Delayed Fluorescence. *Adv. Energy Mater.* **2015**, *5*, 1401770.
- (58) Muccioli, L.; D'Avino, G.; Zannoni, C. Simulation of Vapor-Phase Deposition and Growth of a Pentacene Thin Film on C60(001). *Adv. Mater.* **2011**, *23*, 4532–4536.
- (59) Troisi, A.; Orlandi, G. The Hole Transfer in DNA: Calculation of Electron Coupling between Close Bases. *Chem. Phys. Lett.* **2001**, *344*, 509–518.
- (60) Muñoz-Losa, A.; Curutchet, C.; Galván, I. F.; Mennucci, B. Quantum mechanical methods applied to excitation energy transfer: A comparative analysis on excitation energies and electronic couplings. *J. Chem. Phys.* **2008**, *129*, 034104.
- (61) Di Donato, M.; Iagatti, A.; Lapini, A.; Foggi, P.; Cicchi, S.; Lascialfari, L.; Fedeli, S.; Caprasecca, S.; Mennucci, B. Combined Experimental and Theoretical Study of Efficient and Ultrafast Energy Transfer in a Molecular Dyad. *J. Phys. Chem. C* **2014**, *118*, 23476–23486.
- (62) Hopfield, J. J. Electron Transfer Between Biological Molecules by Thermally Activated Tunneling. *Proc. Natl. Acad. Sci. U.S.A.* **1974**, *71*, 3640–3644.
- (63) Wang, X.-B.; Woo, H.-K.; Wang, L.-S. Vibrational Cooling in a Cold Ion Trap: Vibrationally Resolved Photoelectron Spectroscopy of Cold C60[−] Anions. *J. Chem. Phys.* **2005**, *123*, 051106.
- (64) Rabalais, J. W.; Karlsson, L.; Werme, L. O.; Bergmark, T.; Siegbahn, K. Analysis of vibrational structure and Jahn-Teller effects in the electron spectrum of ammonia. *J. Chem. Phys.* **1973**, *58*, 3370–3372.
- (65) Ricci, G.; Canola, S.; Dai, Y.; Fazzi, D.; Negri, F. Impact of Fluoroalkylation on the n-Type Charge Transport of Two Naphthodithiophene Diimide Derivatives. *Molecules* **2021**, *26*, 4119.
- (66) He, L.; Guo, Y.; Kloo, L. The dynamics of light-induced interfacial charge transfer of different dyes in dye-sensitized solar cells studied by ab initio molecular dynamics. *Phys. Chem. Chem. Phys.* **2021**, *23*, 27171–27184.
- (67) Kupgan, G.; Chen, X.; Bredas, J.-L. Molecular Packing of Non-Fullerene Acceptors for Organic Solar Cells: Distinctive Local Morphology in Y6 Versus ITIC Derivatives. *Materials Today Advances* **2021**, *11*, 100154.
- (68) Deniz Özdemir, A.; Inanlou, S.; Symalla, F.; Xie, W.; Wenzel, W.; Elstner, M. Dynamic Effects on Hole Transport in Amorphous Organic Semiconductors: a Combined QM/MM and kMC Study. *J. Chem. Theory Comput.* **2023**, *19*, 3849–3860.
- (69) Moore, J.; Pearson, R. *Kinetics and Mechanism*; A Wiley-Interscience publication; Wiley, 1981.
- (70) Lee, J.-W.; Sun, C.; Phan, T. N.-L.; Lee, D. C.; Tan, Z.; Jeon, H.; Cho, S.; Kwon, S.-K.; Kim, Y.-H.; Kim, B. J. Trimerized small-molecule acceptors enable high-performance organic solar cells with high open-circuit voltage and prolonged life-time. *Energy Environ. Sci.* **2023**, *16*, 3339–3349.